THE JOURNAL OF BIOLOGICAL CHEMISTRY VOL. 289, NO. 34, pp. 23963–23976, August 22, 2014

NMR-based Structural Analysis of the Complete Rough-type Lipopolysaccharide Isolated from *Capnocytophaga canimorsus*[*]

Received for publication, April 30, 2014, and in revised form, June 25, 2014 Published, JBC Papers in Press, July 2, 2014, DOI 10.1074/jbc.M114.571489

Ulrich Zähringer[‡1], Simon Ittig[§2], Buko Lindner[‡], Hermann Moll[‡], Ursula Schombel[‡], Nicolas Gisch[‡], and Guy R. Cornelis[§¶3]

From the [‡]Division of Immunochemistry/Bioanalytical Chemistry, Research Center Borstel, Leibniz-Center for Medicine and Biosciences, Parkallee 4a, 23845 Borstel, Germany, [§]Infection Biology, Biozentrum, University of Basel, Klingelbergstrasse 50/70, CH-4056 Basel, Switzerland, and the [¶]Department of Biology, University of Namur, B5000 Namur, Belgium

Background: Rough-type LPS of *C. canimorsus* is biologically active, whereas lipid A is not.
Results: Purified *C. canimorsus* rough-type LPS could be analyzed in intact form by NMR.
Conclusion: Inactive lipid A becomes active in case the core oligosaccharide is attached.
Significance: This study provides evidence that lipid A is not the sole part of the LPS structure responsible for endotoxic activity.

We here describe the NMR analysis of an intact lipopolysaccharide (LPS, endotoxin) in water with 1,2-dihexanoyl-*sn*-glycero-3-phosphocholine as detergent. When HPLC-purified rough-type LPS of *Capnocytophaga canimorsus* was prepared, ^{13}C,^{15}N labeling could be avoided. The intact LPS was analyzed by homonuclear (^{1}H) and heteronuclear (^{1}H,^{13}C, and ^{1}H,^{31}P) correlated one- and two-dimensional NMR techniques as well as by mass spectrometry. It consists of a penta-acylated lipid A with an α-linked phosphoethanolamine attached to C-1 of GlcN (I) in the hybrid backbone, lacking the 4′-phosphate. The hydrophilic core oligosaccharide was found to be a complex hexasaccharide with two mannose (Man) and one each of 3-deoxy-D-manno-oct-2-ulosonic acid (Kdo), Gal, GalN, and L-rhamnose residues. Position 4 of Kdo is substituted by phosphoethanolamine, also present in position 6 of the branched Man^{I} residue. This rough-type LPS is exceptional in that all three negative phosphate residues are "masked" by positively charged ethanolamine substituents, leading to an overall zero net charge, which has so far not been observed for any other LPS. In biological assays, the corresponding isolated lipid A was found to be endotoxically almost inactive. By contrast, the intact rough-type LPS described here expressed a 20,000-fold increased endotoxicity, indicating that the core oligosaccharide significantly contributes to the endotoxic potency of the whole rough-type *C. canimorsus* LPS molecule. Based on these findings, the strict view that lipid A alone represents the toxic center of LPS needs to be reassessed.

Capnocytophaga canimorsus is a Gram-negative bacterium of the family *Flavobacteriaceae*, commonly found in the mouths of dogs and causing rare but serious human infections resulting from bites, scratches, or even licks (1–4). The infection rapidly progresses to life-threatening septicemia (5). Although it is not perfectly clear yet why these bacteria can be so aggressive, a number of virulence factors have been described recently. First, *C. canimorsus* bacteria have the unusual capacity to deglycosylate human glycoproteins, including IgGs and cell surface glycoproteins from phagocytes (6–8). In addition, *in vitro*, they resist phagocytosis (2) and killing by complement (9). The lipopolysaccharide (LPS, endotoxin) representing one of the most potent pathogen-associated molecular patterns of Gram-negative bacteria (10) is the key compound to the latter properties (3, 9).

Recently, we analyzed the lipid A structure and function of *C. canimorsus* and identified it as a penta-acylated lipid A, which lacks the 4′-phosphate and carries a phosphoethanolamine (*P*-Etn)[4] in position C-1 of the lipid A backbone (11). It has long been known but seldom been addressed that, besides phosphates and fatty acids, the core oligosaccharide also contributes to an enhanced endotoxicity of the lipid A molecule by 1–2 orders of magnitude (12, 13). By contrast, in *C. canimorsus*, the endotoxicity is enhanced by a factor of 20,000 when the core oligosaccharide is attached to lipid A (11). This is most remarkable because this lipid A contains only five fatty acids and only one phosphate residue attached to the lipid A backbone (13, 14). Which functional group in the lipid A and/or in the prox-

* This work was supported in part by the Cluster of Excellence "Inflammation at Interfaces" (EXC306).
[1] To whom correspondence may be addressed. Tel.: 49-4537-188-4620; Fax: 49-4537-188-7450; E-mail: uzaehr@fz-borstel.de.
[2] Supported by the Werner Siemens Foundation. To whom correspondence may be addressed. Tel.: 41-61-267-2200; Fax: 41-61-267-2118; E-mail: simon.ittig@unibas.ch.
[3] Recipient of European Research Council 5 Grant AdG 2011-293605-CAPCAN.

[4] The abbreviations used are: *P*-Etn, phosphoethanolamine; DHPC, 1,2-dihexanoyl-*sn*-glycero-3-phosphocholine; DHPC-d_{40}, perdeutero-DHPC; ELSD, evaporative light-scattering detector; Gal, galactose; GalN, 2-amino-2-deoxy-D-galactose; GLC, gas-liquid chromatography; GlcN, 2-amino-2-deoxy-D-glucose; GlcN3N, 2,3-diamino-2,3-dideoxy-D-glucose; GPC, gel permeation chromatography; Gro, glycerol; HMBC, heteronuclear multiple-bond correlation; HMQC, heteronuclear multiple quantum coherence; HSQC, heteronuclear single quantum coherence; Kdo, 3-deoxy-D-manno-oct-2-ulosonic acid; Man, mannose; MD-2, myeloid differentiation factor 2; *P*, phosphate; Rha, rhamnose; ROESY, rotating-frame nuclear Overhauser effect spectroscopy; TLR2 and TLR4, Toll-like receptor 2 and 4, respectively; TOCSY, total correlated spectroscopy; Cc5, *C. canimorsus* 5; ESI, electrospray ionization; AMP, antimicrobial peptide.

imal core oligosaccharide of *C. canimorsus* might be able to contribute to this unexpected enhancement in endotoxicity?

To answer this question, we first isolated the LPS-derived oligosaccharides by conventional approaches using (i) acid hydrolysis (leading to core oligosaccharide **1**; Fig. 1) or (ii) strong hydrazinolysis for deacylation of the LPS/lipid A (leading to core backbone oligosaccharide **2**; Fig. 1) and determined the complete structures by ESI-MS and NMR in D_2O. By contrast, when rough-type LPS, which still contains the hydrophobic lipid A moiety, was subjected to NMR analysis, only complex organic solvent mixtures, such as chloroform/methanol/water, were able to give well resolved NMR signals (15). However, conformational studies of the LPS molecule expressing relevant biological (*i.e.* endotoxic active) conformations in an aqueous solvent system cannot be achieved by this approach (16).

Although the acyl chains and phosphates have been proven to be extremely important for the LPS/lipid A structure-function relationship (12, 17, 18), the contribution of the core oligosaccharide has not been considered so far. It is generally accepted that the lipid A represents the endotoxic moiety of the whole LPS molecule (14), and other components, like the inner core oligosaccharide, are often considered to be less or even not important. By contrast, in *C. canimorsus* LPS, we obtained strong evidence that indeed the core oligosaccharide can contribute to its endotoxicity (11). We found that the negatively charged carboxyl group of the Kdo adjacent to the lipid A backbone can replace the function of the 4′-phosphate that is sterically close to it. Therefore, an analytical tool enabling the analysis of the conformation of the core oligosaccharide when attached to the lipid A by NMR in a water mimetic is expected to shed more light onto the LPS structure-function relationship. By this approach, we aimed to explain interactions of intact rough-type LPS with natural pathogen-related receptors (MD-2 and TLR4) under nearly natural conditions, where conformational aspects become important for the understanding of various biological functions.

Here we describe an analytical approach using HPLC purification of *C. canimorsus* rough-type LPS (**3**, Fig. 1) followed by NMR analysis in a water mimetic. This way we could show that not only the primary structure but also the conformation of LPS could successfully be analyzed by NMR spectroscopy, avoiding expensive ^{13}C,^{15}N labeling. Our data give new insights into the conformational flexibility of the core oligosaccharide, which can be helpful to explain the difference between the low activity of free lipid A of *C. canimorsus* on the one hand and the high endotoxic activity of the rough-type LPS on the other (11).

MATERIALS AND METHODS

Bacterial Strains, Growth Conditions, and Extraction of LPS

C. canimorsus 5 (Cc5) (3) and its complement-sensitive Y1C12 mutant (9) were grown on heart infusion agar 5% sheep blood supplemented with gentamicin and, in the case of Y1C12, with erythromycin. The Cc5-based Y1C12 mutant has a transposon insertion within a predicted glycosyltranferase-encoding gene, probably the *N*-acetylfucosamine transferase WbuB, necessary for the formation of the O-antigen (9). Bacteria were harvested by scraping off colonies from the agar surface of 500 plates, washed, and resuspended in PBS. Selective agents were added at the following concentrations: erythromycin, 10 mg/ml; gentamicin, 20 mg/ml.

Bacterial cells were washed with ethanol, acetone, diethylether (500 ml each) and centrifuged to give 11.2 g (Cc5) and 30.8 g (Y1C12) of air-dried bacteria, respectively. Both LPSs were extracted with phenol/water (19), whereby the crude LPS of WT Cc5 was identified in the water, and that of the mutant was identified in the phenol phase. Extraction by the phenol/chloroform/petroleum ether method (20), RNase/DNase treatment (30 mg; Sigma; 24 h at room temperature), proteinase K digestion (30 mg; 16 h at room temperature), extended dialysis (2 days at 4 °C), and lyophilization revealed 188 mg of Cc5 (1.7%, w/w) and 200 mg of Y1C12 LPS (0.6%, w/w). Compositional analysis of the LPS from the WT strain showed it to be highly contaminated with glucose from amylopectin (21), flavolipin (22), and capnin (23, 24), known to be present in *Capnocytophaga* spp. and *Flavobacteriaceae*. In contrast, the LPS from the Y1C12 mutant was devoid of such contaminating material. Because the compositional analysis of the core obtained from the WT strain Cc5 LPS and that of Y1C12 revealed no differences with respect to their sugars and fatty acids, the Y1C12 mutant was considered to be the strain of choice to isolate and analyze the intact rough-type LPS in detail.

Preparation and Purification of 1 after Acid Hydrolysis

LPS isolated from the WT bacteria (25 mg) and Y1C12 mutant (50 mg) was heated in 10 ml of 2% AcOH for 1.5 h at 100 °C. Precipitating lipid A was removed by centrifugation, and the core oligosaccharide in the supernatant was lyophilized and further purified by GPC on a column (2.5 × 120 cm, Toyopearl (HW-40S) Tosoh, Bioscience, Germany), eluted with pyridine/acetic acid/water (8:20:2000, v/v/v, pH ~4.7) at a flow rate of 0.7 ml/min. Oligosaccharides were monitored by a Knauer differential refractometer. Appropriate fractions (7.5 ml) containing the core sugars (as detected by GLC-MS) were collected and lyophilized. The yield of the GPC-purified **1** was 5.8 mg (25%) for the WT strain Cc5 and 12 mg (24%) for the Y1C12 mutant. Compositional analysis by GLC-MS of both core oligosaccharide fractions resulted in identical sugar residues being present in comparable proportions. As expected, the core oligosaccharide fraction of the mutant did not contain contaminating amylopectin (21) and sugars from the O-chain (9). Thus, the Y1C12 mutant was found to be representative for further structural analysis of the complete rough-type *C. canimorsus* LPS (**3**).

Preparation and Purification of 2 after Strong Hydrazinolysis

LPS of the Y1C12 mutant (50 mg) was completely deacylated by strong hydrazinolysis (1.0 ml of N_2H_4, 100 °C, 16 h). The product was precipitated from cold acetone (10 ml) and dried under a stream of nitrogen. Liberated fatty acids were removed from the sediment by repeated extraction from water/chloroform (3 × 15 ml). The combined water phases were centrifuged (15 min, 7,000 rpm, 4 °C) and lyophilized to give 28.7 mg of crude core backbone oligosaccharide, which was further puri-

fied by GPC as described above, whereby a low but acceptable yield (2.2 mg, 4.4% w/w) of **2** was obtained.

Preparation and HPLC Purification of the Intact Rough-type LPS

The rough-type LPS was isolated by chance from an LPS preparation of the Y1C12 mutant (51.3 mg) because mild acetate buffer hydrolysis, which we tried first (0.1 M NaOAc, pH 4.4, containing 1% SDS (25) at 100 °C for 3 h under stirring), did not liberate free lipid A from the core oligosaccharide. Because ESI-MS analysis of this hydrolysate revealed that it still contained a considerable amount of unhydrolyzed and intact rough-type LPS (> 60%), this preparation was considered to be suitable for the purification of compound **3** by preparative HPLC.

To this end, an Abimed-Gilson HPLC system equipped with a semipreparative Kromasil C18 column (5 μm, 100 Å, 10 × 250 mm, MZ-Analysentechnik) was loaded with about 2–5 mg of the crude LPS. Lipid A and LPS fractions were eluted using a gradient of methanol/chloroform/water (57:12:31, v/v/v) containing 10 mM NH_4OAc as mobile phase A and chloroform/methanol (70.2:29.8, v/v) with 50 mM NH_4OAc as mobile phase B. The initial solvent system consisted of 2% B and was maintained for 20 min, followed by a three-step linear gradient rising from 2 to 17% B (20–50 min), from 17 to 27% B (50–85 min), and from 27 to 100% B (85–165 min). The solvent was held at 100% B for 12 min, and the column was re-equilibrated during 10 min to 2% B and held there for an additional 20 min before the next injection. The flow rate for preparative runs was 2 ml/min (~80 bar) using a splitter (~1:35) between the evaporative light-scattering detector (ELSD) and the fraction collector.

The smaller part of the eluate was split by a Sedex model 75C ELSD (S.E.D.E.R.E., Alfortville, France) equipped with a low flow nebulizer. Fractions were collected in 1- and 0.75-min intervals, depending on the peak elution profile. Nitrogen (purity 99.996%) was used as gas to nebulize the post-column flow stream at 3.5 bar into the detector at 50 °C, setting the photomultiplier gain to 9. The detector signal was transferred to the Gilson HPLC Chemstation (Trilution LC, version 2.1) for detection and integration of the ELSD signals.

According to the ELSD detector response, fractions representing the three main peaks in the HPLC chromatogram (Fig. 2) were combined. From one injection (5 mg of hydrolyzed LPS) the following pools were obtained: pool 1 (70–77 min, yield 0.81 mg, 16%), pool 2 (79–90 min, yield 1.45 mg, 30%), and pool 3 (115.5–118 min, yield 0.62 mg, 12%). Besides the LPS of Y1C12, containing a short O-chain oligosaccharide (data not shown), ornithine lipids (30), capnin (24), flavolipin (31), and other lipids were identified in pool 1. The main fraction (pool 2, yield 1.45 mg) (Fig. 2) represented the purified and complete rough-type LPS of *C. canimorsus* (**3**). The third fraction, pool 3 (yield 0.62 mg), was free lipid A as determined by ESI-MS ([M] = 1717.308 units). Its structural analysis and exceptional biological properties have been described elsewhere (11).

Analytical Procedures

SDS-PAGE—SDS-PAGE of LPS isolated from the WT strain Cc5 and the Y1C12 mutant was run on 18% polyacrylamide gel (26) and silver-stained as described (27).

GLC-MS Analysis—Sugar and fatty acid derivatives were analyzed by GLC-MS on a 5975 inert XL Mass Selective Detector (Agilent Technologies) equipped with a 30-m HP-5MS column (Hewlett-Packard) using a temperature gradient of 150 °C (3 min) → 320 °C at 5 °C/min.

Compositional and Methylation Analyses—Compositional analysis was done by GLC-MS. Glycolipid and oligosaccharide samples (0.1 mg) were subjected to methanolysis (0.5 M HCl/MeOH, 45 min, 85 °C) and per-*O*-acetylated (15 μl of pyridine, 15 μl of Ac_2O, 85 °C, 15 min). The configuration of the aldopyranosides was confirmed by GLC of acetylated (*R*)-2-octyl glycosides (28), whereby Rha was found to be L-configured and all other sugars D-configurated. Methylation analysis of the isolated core oligosaccharides was carried out after *N*-acetylation (Ac_2O/NaOH) (29), HF treatment (48% aqueous HF, room temperature, 2 h), permethylation, hydrolysis (2 M TFA at 100 °C at 1.5 h and/or 4 M TFA at 100 °C for 6 h), reduction ($NaBD_4$) and per-*O*-acetylation followed by GLC-MS analysis.

ESI-Mass Spectrometry—ESI-MS analyses of compounds **1**, **2**, and **3** were performed in the negative ion mode on a high resolution Fourier transform ion cyclotron resonance mass spectrometer (Apex Qe, Bruker Daltonics, Billerica, MA), equipped with a 7-tesla superconducting magnet and an Apollo dual ESI/MALDI ion source. Sample preparation and instrumental settings were recorded as described previously (11).

NMR Spectroscopy—The NMR spectra of oligosaccharides **1** and **2** were recorded at 300 K on a Bruker 600-MHz (Avance^{II}) NMR spectrometer equipped with a 5-mm quadruple resonance (^1H,^{13}C,^{15}N,^{31}P) probe with *Z*-gradient. Samples were dissolved in 0.75 ml of D_2O (99.9% D, Cambridge Isotopes, Andover, MA) and lyophilized twice, and spectra were recorded in 0.50 ml of D_2O (99.98% D). Signals were referenced to internal acetone (δ_H 2.225 ppm, δ_C 30.89 ppm), and Bruker standard software xwinnmr (version 3.5) was used to acquire and process these data.

NMR spectroscopic measurements of **3** were performed on a Bruker Avance^{III} 700-MHz spectrometer equipped with an inverse 5-mm quadruple resonance Z-Grad cryoprobe (or with an inverse 1.7-mm triple resonance Z-Grad microcryoprobe). HPLC-purified compound **3** was dissolved in 25 mM deuterated sodium phosphate buffer (pH 6.8) containing 1.5% (w/v) DHPC-d_{40} (98% D, Cambridge Isotopes) and transferred to 5-mm Shigemi (1.3 mg in 325 μl) or 1.7-mm NMR microtubes (0.25 mg in 40 μl) (Bruker), depending on the sample material available. Spectra were recorded under conditions described earlier (32) with minor modifications. Elevated temperatures (325 K) for increasing spectral resolution and lower concentration of the detergent were used. ^1H,^{13}C signals were referenced via selected internal DHPC-d_{40} signals (H-2/C-2^{Gro}; δ_H 5.27 ppm, δ_C 71.4 ppm) after external calibration with acetone (δ_H 2.225 ppm, δ_C 30.89 ppm) recorded under identical conditions. Signals of the H-3^{Gro} in DHPC-d_{40} have been chosen to reference the ^1H,^{31}P HMQC NMR spectra, whereas the one-dimen-

sional ^{31}P NMR spectra were referenced to external aqueous 85% H_3PO_4 (δ_P 0.0 ppm). A mixing time of 200 ms was used in ROESY experiments. For the one-dimensional ^1H NMR spectra, shown as projections of the F_2 axis, the FID signal was multiplied by a Gaussian function (exponential broadening factor −2 Hz, Gaussian broadening factor 0.2 Hz) prior to Fourier transformation. ^1H NMR assignments were confirmed by two-dimensional $^1H,^1H$ COSY and TOCSY experiments, and ^{13}C NMR assignments were done by two-dimensional $^1H,^{13}C$ HSQC, based on the ^1H NMR assignments. Interresidual connectivity and further evidence for ^{13}C assignment were obtained from two-dimensional $^1H,^{13}C$ heteronuclear multiple-bond correlation and $^1H,^{13}C$ HSQC-TOCSY. Connectivity of phosphate groups was assigned by two-dimensional $^1H,^{31}P$ HMQC and $^1H,^{31}P$ HMQC-TOCSY. Bruker software Topspin version 3.1 was used to acquire and process these data.

RESULTS

The Core Oligosaccharide in the Y1C12 Mutant Is Representative of Rough-type C. canimorsus 5 WT LPS—The LPS isolated from the Y1C12 mutant was chosen for the structural analysis of the core oligosaccharide for reasons given below. SDS-PAGE analysis (data not shown) revealed that both WT and Y1C12 mutant contained a significant amount of rough-type LPS. In order to confirm the results obtained by SDS-PAGE, we performed compositional analysis of the core oligosaccharides from both LPS preparations (WT and mutant). They were prepared by acid hydrolysis in 2% AcOH followed by GPC under identical conditions and analyzed separately. Upon GLC-MS analysis, the core oligosaccharide fractions obtained from both strains showed the same retention time upon GPC, and no differences in their composition and proportions of sugars appeared. Both core structures were found to be composed of the same monosaccharides, suggesting that they are identical in both strains due to their genetic relationship. The only difference was the presence of components in the WT Cc5 LPS originating from the O-chain, which eluted prior to the core oligosaccharide (data not shown). As expected, the Y1C12 mutant gave better yield and higher purity for the core oligosaccharide preparation; therefore, the structural analysis described here has been performed with compounds isolated from the mutant, which was regarded to be representative of *C. canimorsus* LPS.

*Isolation and Structural Analysis of the Core Oligosaccharide (**1**)*—To investigate the structure of the core oligosaccharide, LPS of the Y1C12 mutant was hydrolyzed in AcOH, and the core oligosaccharide was purified by GPC. The core oligosaccharide was further analyzed by GLC-MS, ESI-MS, and NMR spectroscopy as described below. Earlier eluting higher molecular fractions contained minor amounts of sugars derived from the O-chain. GLC-MS analysis of the core oligosaccharide (methanolysis, per-*O*-acetylation) revealed the following monosaccharides: Rha, Gal, GalN, and Man in molar ratios of ~1:1:1:2. Kdo and *P*-Etn could not be determined and/or quantified using this methodology.

The charge-deconvoluted ESI-MS spectrum of the core oligosaccharide sample recorded in the negative ion mode showed two major peaks, one having a mass of 1321.384 units, which was assigned to the intact core oligosaccharide composed of 3 hexoses, 1 hexosamine, 1 deoxyhexose, and 1 Kdo with two *P*-Etn residues (calc: 1321.335 units) being in full agreement with structure **1** (Fig. 1). The second major peak (1158.338 units) was identified to originate from **1** after loss of phosphoethanolamine and water (**1**-(*P*-Etn-H_2O)) (calc.: 1158.334 units).

To determine the linkages and substitution pattern, **1** was subjected to methylation analysis. Two partially methylated sugar alditol acetates were identified, 2,3,4-Me_3-Rha-ol and 3,4,6-Me_3-GalNAc-ol, indicating that Rha and GalN represent two terminal sugar residues. Other sugars in the chain were 2,4,6-Me_3-Gal-ol (1,3-linked Gal), 2,3,4-Me_3-Hex-ol (1,6-linked hexose), and 2,6-Me_2-Hex-ol (1,3,4-linked hexose). No sugar fragments of the Kdo were identified because these Kdo derivatives rapidly decompose under the conditions used.

The structure of the core oligosaccharide was further analyzed in detail by homo- and heteronuclear one- and two-dimensional NMR spectroscopy. Complete ^1H and ^{13}C signal assignments are given in Table 1. With the exception of β-Gal (δ_H 4.54 ppm, $J_{1,2}$ 8.1 Hz), all sugars were found to be present in α-linkage because their anomeric protons (H-1) resonate in the range between δ_H 5.0 and 5.26 ppm. The linkages between all sugars in **1** could be completely determined by ROESY and HMBC experiments (Table 2). The connectivity between H-1 of α-GalN (δ_H 5.21 ppm) and H-6a/H-6b of Man^{II} (at δ_H 3.65/4.16 ppm) in the ROESY spectrum was indicative of the α-(1→6) linkage of the terminal GalN in agreement with the data of the methylation analysis. The anomeric proton of the second terminal Rha sugar residue (H-1, δ_H 5.01 ppm) showed NOE cross correlation to H-3 of Gal (δ_H 3.73 ppm). The 3-substituted Gal and the 6-substituted Man^{II} were found both to be linked to the same sugar residue, namely Man^I, thus representing a branching point in the core oligosaccharide. This was deduced from H-1 of β-Gal (δ_H 4.54 ppm) showing a strong and significant NOE to H-4 of Man^I (δ_H 4.25 ppm) for one branch and from H-1 of Man^{II} (δ_H 5.26 ppm) showing an intense NOE to H-3 of Man^I (δ_H 4.17 ppm) representing the second branch. Taken together, the first mannose (Man^I) is disubstituted: in position 3 with α-D-GalN-(1→6)-α-D-Man^{II}-(1→ and in position 4 with α-L-Rha-(1→3)-β-D-Gal-(1→ (Fig. 1). The last anomeric NOE signal of H-1 (Man^I, δ_H 5.05 ppm) showed a connectivity to H-5 (δ_H 4.24 ppm) of Kdo, which represents the "reducing end" of **1** with Kdo being exclusively in the α-anomeric form. All assignments of the NOE signals were further corroborated by data obtained from the HMBC spectrum (Table 2). The positions of the two *P*-Etn residues in **1** were identified from the chemical shifts of the carbon resonances in the HSQC spectrum (Table 1) in which the signal of Kdo H-4 was shifted to lower field due to substitution with *P*-Etn (δ_H 4.50 ppm/δ_C 72.2 ppm). The same observation was made for Man^I H-6 (δ_H 4.22, 4.31 ppm/δ_C 64.9 ppm), which also is *P*-Etn-substituted. In addition, these signals showed cross-peaks in the $^1H,^{31}P$ HMQC and $^1H,^{31}P$ HMQC-TOCSY (Table 3) spectra, further corroborating this interpretation.

*Isolation and Structural Analysis of the Core Backbone Oligosaccharide (**2**)*—Strong hydrazinolysis was used to isolate the core oligosaccharide with the lipid A backbone disaccharide attached. The oligosaccharide obtained from the completely

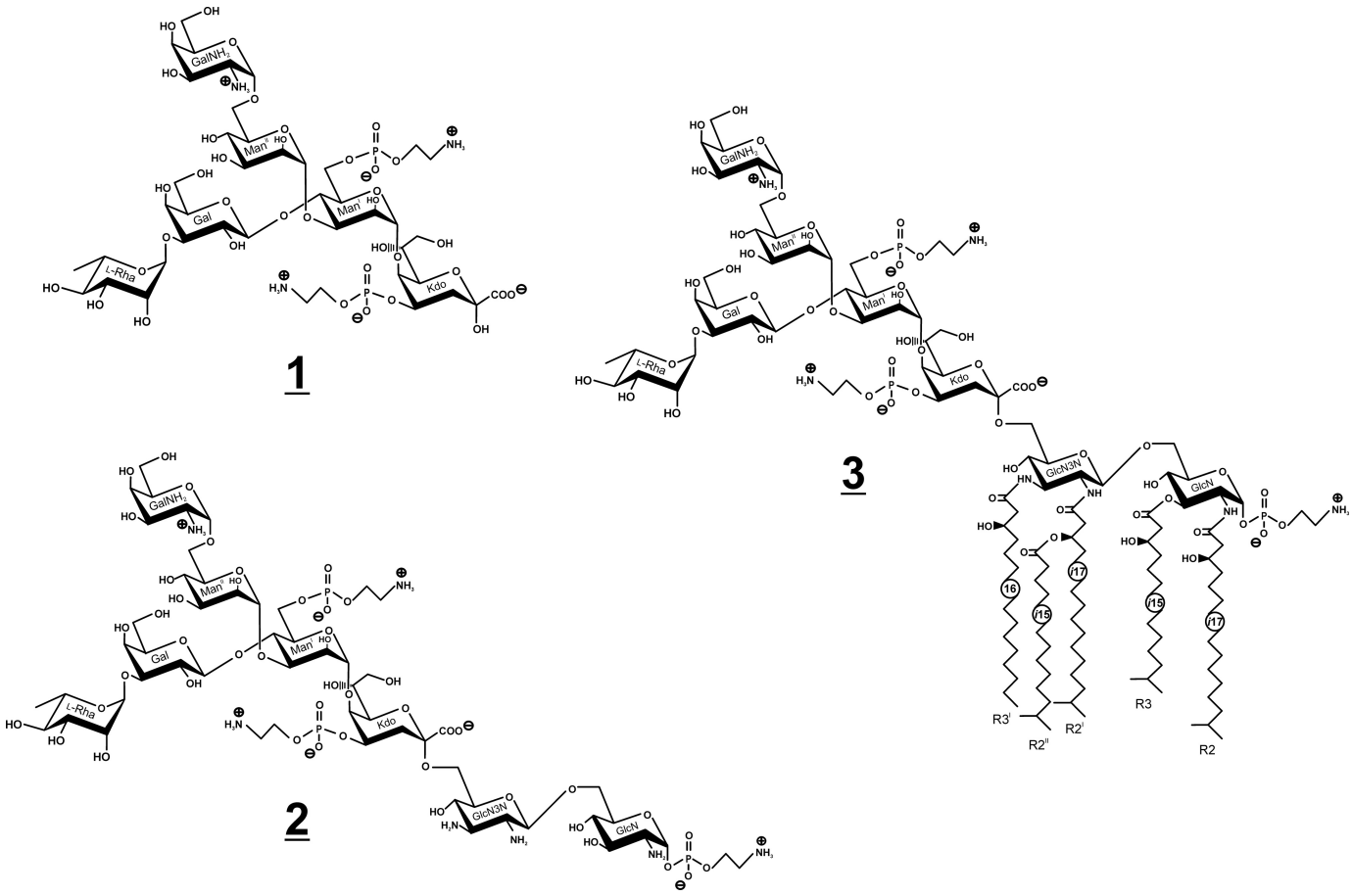

FIGURE 1. **LPS and part structures of *C. canimorsus*.** Shown are structures of the core hexasaccharide (**1**) obtained after acid hydrolysis (AcOH), isolated core backbone octasaccharide (**2**) obtained after strong hydrazinolysis (N_2H_4), and the complete rough-type LPS (**3**).

deacylated LPS (50 mg) was purified by GPC. It resulted in **2** (Fig. 1) in low but acceptable yield. By using negative ion mode ESI-MS, an octasaccharide was identified consisting of Hex_3-$(HexN)_2$-HexN3N-dHex-Kdo (found 1721.537 u; calc. for $C_{56}H_{106}O_{47}N_7P_3$ 1721.517 units) corresponding to structure **2**. The HSQC data of **2** are given in Table 1. Again, with the exception of β-Gal (δ_H 4.52 ppm, $J_{1,2}$ 8.2 Hz, δ_C 104.1 ppm) and GlcN3N (δ_H 4.47 ppm, $J_{1,2}$ 8.0 Hz, δ_C 104.5 ppm), all sugars were found to be α-linked. ROESY and HMBC experiments showed identical linkages as identified in the NMR spectra of the hexasaccharide **1** described above. The structural difference between **1** and **2** is the presence of the lipid A backbone [β-D-Glc*p*N3N-(1′→6)-α-D-Glc*p*N-1-*P*-Etn] to which the core oligosaccharide (**1**) is attached (at position 6′ of Glc*p*N3N).

The positions of the three *P*-Etn-residues were identified from the chemical shifts of the carbon resonances in the HSQC spectrum as well as by $^1H,^{31}P$ HMQC and $^1H,^{31}P$ HMQC-TOCSY spectra (Tables 1 and 3). The third phosphate was found attached to the lipid A hybrid backbone as *P*-Etn residue at GlcN C-1 (H-1/C-1 δ_H 5.49 ppm/δ_C 96.3 ppm). The typical dd signal of H-1 at GlcN (I) showed two coupling constants, one ($^3J_{1,2}$ 3.4 Hz) indicating α-configuration and the second ($^3J_{1,P}$ 6.8 Hz) characteristic of the α-anomeric phosphate substitution in the lipid A backbone (33). Furthermore, a weak NOE signal could be identified between GlcN H-1 (δ_H 5.49 ppm) and H-1a,b, the methylene protons of H-1a,b-*P*-Etn (δ_H 4.15, 4.11 ppm) (Table 1), indicating that *P*-Etn is α-glycosidically bound to C-1 of GlcN of the lipid A hybrid backbone (11).

Isolation and Structural Analysis of the Intact Rough-type LPS—The intact rough-type LPS (**3**) (Fig. 1) was obtained from the LPS preparation of the Y1C12 mutant by preparative HPLC (Fig. 2). As mentioned above, this rough-type LPS represents a significant molecular species present in the native WT LPS. The HPLC analysis of the mild acetate buffer-treated LPS resulted in three major fractions (pools 1, 2, and 3) (Fig. 2). Pool 2 was found to contain the intact rough-type LPS (**3**) and was further analyzed by MS and NMR, as described here in more detail. The other pools were identified as crude and contaminated S-form LPS (pool 1) and lipid A (pool 3), respectively, the analysis and structure of which is described elsewhere (11).

The ESI-MS spectrum of **3** is shown in Fig. 3. The LPS is composed of a hexasaccharide (**1**) (Fig. 1) with a penta-acylated lipid A attached, this way representing a rough-type LPS. The molecular mass identified (found: 2976.680 units; Fig. 3) was in full agreement with the structure **3**, being composed of Hex_3-(HexN)-dHex-Kdo with two *P*-Etn residues in the core and the complete penta-acylated lipid A with one *P*-Etn at the C-1 of GlcN in the hybrid lipid A backbone (11) (calc. for $C_{136}H_{256}O_{56}N_7P_3$ [M] = 2976.661 units and [M + Na] = 2998.639 units). The ESI-MS of **3** also showed further heterogeneity in the acylation of the lipid A (*i.e.* the chain length of the fatty acids differing by one or two methylene group(s)) (-CH_2-,

TABLE 1

^{1}H and ^{13}C NMR data of the isolated core oligosaccharide (1), core backbone oligosaccharide (2), and rough-type LPS (3) from the *C. canimorsus* Y1C12 mutant

Compounds **1** and **2** were measured in D_2O (300 K), whereas **3** was recorded in 25 mM Na-*P* buffer, pH 6.8, containing 1.5% DHPC-d_{40} at 325 K. For further details, see "Materials and Methods." n.d., not determined.

	^{1}H			^{13}C			
Proton	δ_H (ppm) ($J_{n,n+1}$ [Hz])			Carbon	δ_C (ppm)		
	1	**2**	**3**		**1**	**2**	**3**
Residue							
α-D-Gal*p*N-(1→							
H-1	5.21 (3.6)	5.22	5.25	C-1	96.7	96.8	96.8
H-2	3.51 (7.8)	3.45	3.51	C-2	52.3	52.1	52.3
H-3	4.10	4.10	4.10	C-3	68.0	68.1	66.1
H-4	3.99	3.99	3.95	C-4	69.5	69.5	69.1
H-5	3.99	3.96	4.02	C-5	72.7	72.6	72.5
H-6a	3.73	3.70	3.76	C-6	62.4	62.3	62.2
H-6b	3.73	3.74	3.76				
→6)-α-D-Man*p*^{II}-(1→							
H-1	5.26 (<1.0)	5.21	5.24	C-1	103.3	103.2	103.0
H-2	4.18	4.15	4.18	C-2	70.9	70.9	70.8
H-3	3.84	3.83	3.88	C-3	71.9	71.8	71.8
H-4	3.89	3.87	3.90	C-4	67.2	67.1	67.2
H-5	3.82	3.82	3.74	C-5	72.8	72.7	73.4
H-6a	3.65	3.64	3.66	C-6	66.5	66.5	64.9
H-6b	4.16	4.14	4.18				
α-L-Rha*p*-(1→							
H-1	5.01 (1.5)	4.98	5.03	C-1	103.6	103.6	103.3
H-2	4.04	4.00	4.07	C-2	71.4	71.2	71.3
H-3	3.80	3.78	3.82	C-3	71.4	71.0	71.2
H-4	3.43 (9.8)	3.40	3.45	C-4	73.3	73.2	73.2
H-5	3.79 (9.9)	3.75	3.84	C-5	70.5	70.7	70.4
H-6	1.25	1.22	1.27	C-6	17.8	17.8	17.6
→3)-β-D-Gal*p*-(1→							
H-1	4.54 (8.1)	4.52 (8.2)	4.57	C-1	104.2	104.1	103.9
H-2	3.55	3.51	3.57	C-2	72.1	72.0	72.0
H-3	3.73	3.71	3.73	C-3	81.4	81.4	81.2
H-4	3.98	3.99	3.95	C-4	70.0	69.4	69.0
H-5	3.69	3.66	3.70	C-5	76.6	76.5	76.2
H-6a	3.71	3.76	3.81	C-6	62.8	62.6	62.4
H-6b	3.79	3.76	3.81				

TABLE 1—*continued*

	^{1}H			^{13}C			
Proton	δ_H (ppm) ($J_{n,n+1}$ [Hz])			Carbon	δ_C (ppm)		
	1	**2**	**3**		**1**	**2**	**3**
Residue							
→3,4)-α-D-Man*p*^{I}-(1→							
H-1	5.05 (1.4)	5.05	5.09	C-1	101.9	101.7	101.6
H-2	4.08	4.07	4.12	C-2	71.6	71.3	71.3
H-3	4.17	4.09	4.13	C-3	75.7	76.1	76.3
H-4	4.25	4.21	4.24	C-4	74.8	74.4	74.3
H-5	4.27 (2.9)	4.24	4.25	C-5	72.3	72.2	71.9
H-6a	4.22 (11.1)	4.17	4.22	C-6	64.9	64.6	64.6
H-6b	4.31	4.26	4.32				
→4,5)-α-Kdo-(2→							
H-3$_{ax}$	1.96 (12.9)	2.03 (12.6)	2.06 (n.d.)	C-2**	n.d.	n.d.	n.d.
H-3$_{eq}$	2.29 (4.2)	2.17 (4.4)	2.21 (n.d.)	C-3	34.9	35.3	35.2
H-4	4.50	4.52	4.56	C-4	72.2	71.9	71.9
H-5	4.24	4.22	4.23	C-5	75.1	74.4	74.5
H-6	3.88	3.82	3.87	C-6	72.6	72.7	72.9
H-7	3.63	3.73	3.77	C-7	70.6	70.4	70.7
H-8a	3.63	3.61	3.64	C-8	64.4	64.6	64.9
H-8b	3.77	3.88	3.94				
→6)-β-D-Glc*p*N3N-(1→							
H-1	-	4.47 (8.0)	4.62	C-1	-	104.5	104.2
H-2	-	2.61	4.04	C-2	-	56.5	55.9
H-3	-	2.79	3.77	C-3	-	58.6	55.0
H-4	-	3.43	3.48	C-4	-	70.4	69.9
H-5	-	3.54	3.67	C-5	-	75.7	76.6
H-6a	-	3.53	3.58	C-6	-	62.9	64.5
H-6b	-	3.59	3.64				
→6)-α-D-Glc*p*N-(1→*P*-Etn							
H-1	-	5.49 (3.4)[&]	5.43	C-1	-	96.3	95.2
H-2	-	2.90	4.00	C-2	-	55.9	53.0
H-3	-	3.39	5.27	C-3	-	75.8	71.8
H-4	-	3.77	3.76	C-4	-	70.2	67.8
H-5	-	3.97	3.97	C-5	-	73.7	73.0
H-6a	-	3.80	4.00	C-6	-	70.4	69.1
H-6b	-	4.15	4.25				
P-Etn- (→6-Man^{I}, →4-Kdo, GlcN-1→)							
H-1 a,b^{Kdo,Man}		(**1**)	4.12, 4.14	C-1	63.3, 63.3		
H-1 a,b^{Kdo,Man}		(**2**)	4.11, 4.11, 4.07	C-1	62.0, 62.0, 61.8		
H-1 a,b^{Kdo,Man,GlcN}		(**3**)	4.15, 4.11, 4.11	C-1	63.1, 63.0, 63.0		
H-2 a,b^{Kdo,Man}		(**1**)	3.29*	C-2	41.4		
H-2 a,b^{Kdo,Man}		(**2**)	3.24*	C-2	40.0		
H-2 a,b^{Kdo,Man}		(**3**)	3.29*	C-2	41.3, 41.3		
H-2 a,b^{GlcN}		(**3**)	3.26	C-2	41.3		

[&] $^3J_{1,P}$ (6.8 Hz).
* Non-resolved multiplet.
** Lacking due to assignment by HSQC.

$\Delta m/z = 14$ units), which was also previously found in the free lipid A (11).

The HPLC purification of *C. canimorsus* rough-type LPS (**3**) revealed a degree of purity sufficient for structural and conformational studies using high-field NMR spectroscopy without ^{13}C,^{15}N-labeling. To this end, homonuclear two-dimensional techniques (COSY, TOCSY, and ROESY) and heteronuclear two-dimensional spectra ^{1}H,^{13}C HSQC, ^{1}H,^{13}C HMBC, ^{1}H,^{31}P HMQC, and ^{1}H,^{31}P HMQC-TOCSY of compound **3** in small DHPC-d_{40} micelles could be obtained with rather good resolution of all signals (Fig. 4). Fig. 5 shows the most complex but well resolved part of the ^{1}H,^{13}C HSQC spectrum of **3** in more detail. Because water was used as solvent, sugar resonances and assignments of the glycolipid can be compared directly with those of the deacylated and purified oligosaccharides **1** and **2** representing partial structures of this LPS (Table 1). The terminal (non-reducing) part of both oligosaccharides (**1** and **2**) had almost identical chemical shifts and coupling constants when compared with those of the native rough-type LPS (**3**). Notably, ^{1}H,^{13}C signals from atoms of the hybrid lipid A backbone (Glc*p*N3N-Glc*p*N disaccharide) embedded in the micellar membrane (Table 1) as well as the signals of the fatty acids (Table 4) were well resolved in the HSQC spectrum of **3** (Figs. 4–6). However, as can be seen in Fig. 5, the ring protons/carbons of the lipid A backbone appear significantly reduced (~50% of intensity) as compared with those obtained from the core oligosaccharide due to an impaired flexibility and resultant line broadening in the NMR spectrum. Despite the fact that the peak resolution of signals obtained from compound **3** were slightly reduced, some diagnostic ^3J-coupling constants in the flexible core oligosaccharide could nevertheless be identified (Fig. 5 and Table 1). For the complete assignment of the HSQC spectrum of **3**, data obtained from oligosaccharides **1** and **2** were extremely helpful. Especially the assignment of positions of the charged, zwitterionic *P*-Etn residues could be determined by changes in the chemical shift values and by the NOE connectivities (Tables 1 and 2). Of note is the fact that all negatively charged phosphate residues were found to be "neutralized" by positively charged ethanolamine groups (P-O-CH_2-CH_2-NH_3^+). This fact holds true not only for the three *P*-Etn residues but also for the carboxyl group of Kdo, which is "neutralized" by the positively charged Gal*p*NH_3^+ residue in the core oligosaccharide when considering the complete rough-type LPS structure of the Y1C12 mutant.

TABLE 2

NOE and HMBC connectivities for compounds 1, 2, and 3

NOEs were classified into strong (s), medium (m), weak (w), and very weak (vw) after calibration to intraresidual NOEs (not listed in this table, except H-3 for Kdo (§). n.d., not detectable.

		Correlation to atom (from anomeric proton§)	
		NOE	HMBC
Sugar residue			
Core hexasaccharide (1)			
→5)-α-Kdo-(2→	H-3_{ax}	(n. d.)	
	H-3_{eq}	H-5Man^{I} (w)	
→3,4)-α-D-Man*p*^{I}-(1→		H-5 Kdo (s)	C-5 Kdo
→6)-α-D-Man*p*^{II}-(1→		H-3 Man^{I} (s)	C-3 Man^{I}
→3)-β-D-Gal*p*-(1→		H-4 Man^{I} (s)	C-4 Man^{I}
α-L-Rha*p*-(1→		H-3 Gal (m)	C-3 Gal
α-GalN*p*-(1→		H-6a,6b Man^{I} (s,w)	C-6 Man^{II}
Core backbone octasaccharide (2)			
→6)-α-D-Glc*p*N-(1→*P*-Etn		1-*P*-Etn H-1a,b (vw)	n.d.
→6)-β-D-Glc*p*N3N-(1→		H-6a,6b GlcN (m,m)	n.d.
→5)-α-Kdo-(2→	H-3 $_{ax}$	H-3 Man^{I} (w), H-5 Man^{I} (m)	n.d.
	H-3 $_{eq}$	H-3 Man^{I} (w)	
→3,4)-α-D-Man*p*^{I}-(1→		H-5 Kdo (s)	C-5 Kdo
→6)-α-D-Man*p*^{II}-(1→		H-3 Man^{I} (s)	C-3 Man^{I}
→3)-β-D-Gal*p*-(1→		H-4 Man^{I} (s)	C-4 Man^{I}
α-L-Rha*p*-(1→		H-3 Gal (s)	C-3 Gal
		H-4 Gal (s)	
		H-2 Gal (w)	
α-D-GalN*p*-(1→		H-6a,6b Man^{I} (s,m)	C-6 Man^{II}
rough-type LPS (3) in DHPC-d_{40} micelles			
→6)-α-D-Glc*p*N-(1→*P*-Etn		H-1a,b *P*-Etn (w)	
		H-2a,b *P*-Etn (w)	
→6)-β-D-Glc*p*N3N-(1→		H-6a,6b α-D-Glc*p*N (s,s)	
→5)-α-Kdo-(2→	H-3_{ax}	H-3 Man^{I} (w), H-5 Man*p*^{I} (vw)	
	H-3_{eq}	n.d.	
	H-4	H-1a,b-*P*-Etn (w)	
		H-2a,b-*P*-Etn (w)	
→3,4)-α-D-Man*p*^{I}-(1→		H-5 Kdo (s), H-7 Kdo (m), H-8a Kdo (w)	
		H-2a,b *P*-Etn (w)	
→6)-α-D-Man*p*^{II}-(1→		H-3 Man*p*^{I} (m), H-2 Gal*p* (w)	
→3)-β-D-Gal*p*-(1→		H-4 Man*p*^{I} (m)	
α-L-Rha*p*-(1→		H-3 Gal*p* (m), H-2 Gal*p* (w), H-4 Gal*p*N (w)	
		H-2a,b *P*-Etn (w)	
α-D-GalN*p*-(1→		H-6a,6b Man*p*^{II} (s,s)	
		H-1a,1b *P*-Etn (w)	

TABLE 3

^{31}P NMR (283.7 MHz) data of compounds 1, 2, and 3

	^{31}P δ (ppm)		
	1	**2**	**3**
Residue			
GlcN→1-*P*-Etn	-	-0.89	- 1.24
6-*P*-Etn-Man^{I}-(1→	0.22	0.15	0.32
4-*P*-Etn-Kdo-(2→	-0.53	0.90	- 0.47

^{31}P signal resonances were assigned according to ^{1}H,^{31}P HMQC and ^{1}H,^{31}P HMQC-TOCSY spectroscopy.

Concerning substitution of the phosphate residues, all three were present in the form of *P*-Etn attached to the core backbone oligosaccharide. The resonances of the H-6a,b/C-6 signals of Man^{I} could be clearly distinguished from the unsubstituted H-6a,b/C-6 signals of Man attached to Kdo (34). Man^{I} signals at δ_H 4.32 and 4.22 ppm/C-6: δ_C 64.6 ppm indicated the 6-position to be substituted by *P*-Etn. The assignment of the *P*-Etn residue resulted from a weak NOE signal of α-Man^{I} (H-1 δ_H 5.09 ppm) to -CH_2-NH_3^+ of *P*-Etn (H-2a,b δ_H 3.29 ppm) (Table 3).

The second phosphate in **3** was found attached to C-4 of Kdo (H-4/C-4 δ_H 4.56 ppm/δ_C 71.9 ppm). Its position was deduced from a weak NOE signal identified between Kdo H-4 and H-1a,b (δ_H ~4.11 ppm) as well as H-2a,b (δ_H ~3.29 ppm), both representing methylene protons of the Etn residue attached to the 4-*P* of Kdo.

The third phosphate was found to be linked to C-1 of the lipid A backbone GlcN (H-1/C-1 δ_H 5.43 ppm/δ_C 95.2 ppm). Its position was deduced from a weak NOE signal identified between GlcN H-1 (δ_H 5.43 ppm) and the methylene protons H-1a,b (δ_H ~4.15 ppm) of 1-*P*-Etn (Table 1), indicating that *P*-Etn was α-glycosidically bound to C-1 of GlcN of the lipid A hybrid backbone (11).

Two-dimensional ^{1}H,^{31}P NMR spectra (HMQC and HMQC-TOCSY) were used to analyze all phosphate positions in more detail. Despite the disadvantage that the ^{31}P signals of the phosphate buffer (25 mM) and DHPC-d_{40} detergent (3.3 mM) were more intense, compared with phosphate signals of **3** (1.3 mM), the HMQC-TOCSY spectra allowed us to assign all signals from the individual sugar residues unequivocally (Table 1).

The ROESY spectrum of **3** revealed correlations of the anomeric protons between all sugars by which substitution and sequence of the complete core oligosaccharide could be determined (Fig. 7). Comparison with those ROESY signals of the oligosaccharides **1** and **2**, lacking the fatty acids of the lipid A, revealed identical but also different conformations (Table 2). Of utmost interest was the structural and conformational analysis of compound **3**. It deserves special mention that some selected ROESY signals identified there were lacking in **1** and **2** and vice versa.

Of special note is one specific conformation expressed by the core oligosaccharide in **3**, which was only observed in this compound. Here weak but detectable NOE signals between the axial proton of Kdo (H-3_{ax}) above and those two axial protons in Man^{I} (H-3 and H-5) below the pyranose ring indicate a significant rotational freedom around the C1-Man^{I}-O-C5-Kdo bond in the core oligosaccharide (Fig. 8). This is unexpected because the glycolipid part of the rough-type LPS is embedded into the micellar membrane of DHPC-d_{40}, resulting in a steric hindrance of the free rotation around this bond between Man^{I} and Kdo.

DISCUSSION

The structural analysis of a complex glycolipid by NMR in water described here represents the first example of a natural abundant highly purified intact rough-type LPS embedded in small micelles in a water mimetic. Such NMR spectra could so far only be obtained with expensive ^{13}C,^{15}N-labeled rough-type LPS (32). The high purity of the LPS preparation permits the use of NMR spectroscopy for a thorough and complete analysis of not only the primary but also the secondary structure (*i.e.* the conformation of natural abundant LPS molecules when present in water). It is well documented that the conformations of LPS are critical for the interaction with its biological partners, initial binding proteins (LBP (36) and CD14 (37)) and also with the final target receptors (MD-2/TLR4 (17)). Using the approach described here, LPS conformational analysis now becomes accessible for its investigation in water, which cannot be analyzed by x-ray crystallography due to the extreme high flexibility of the sugars of the core oligosaccharides (17).

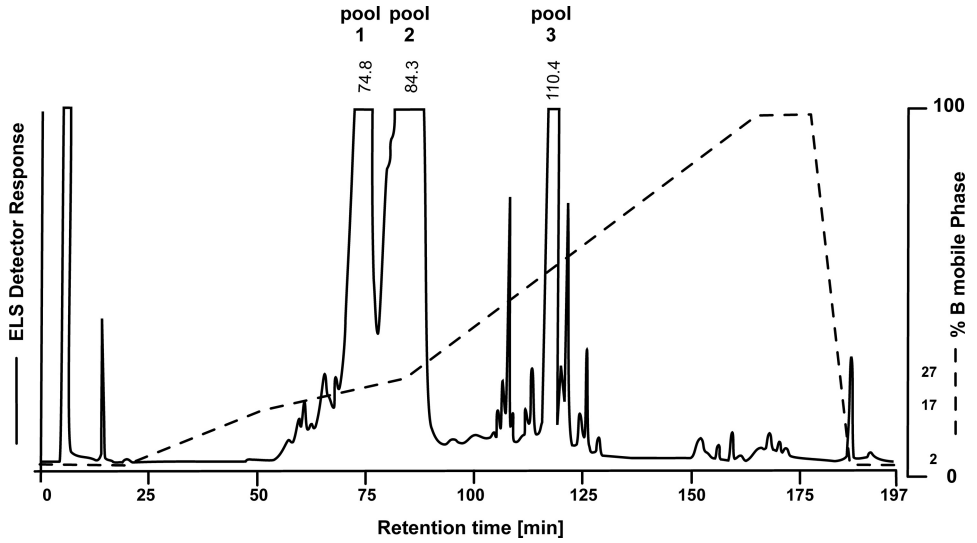

FIGURE 2. **Reversed phase HPLC profile obtained from the *C. canimorsus* Y1C12 mutant LPS after mild acetate buffer hydrolysis.** Note that only ~10% of the free lipid A (pool 3) was obtained under the conditions used, whereas the intact rough-type LPS (**3**, pool 2) predominated (>60%) and could be separated to homogeneity. *ELS Detector*, evaporative light-scattering detector.

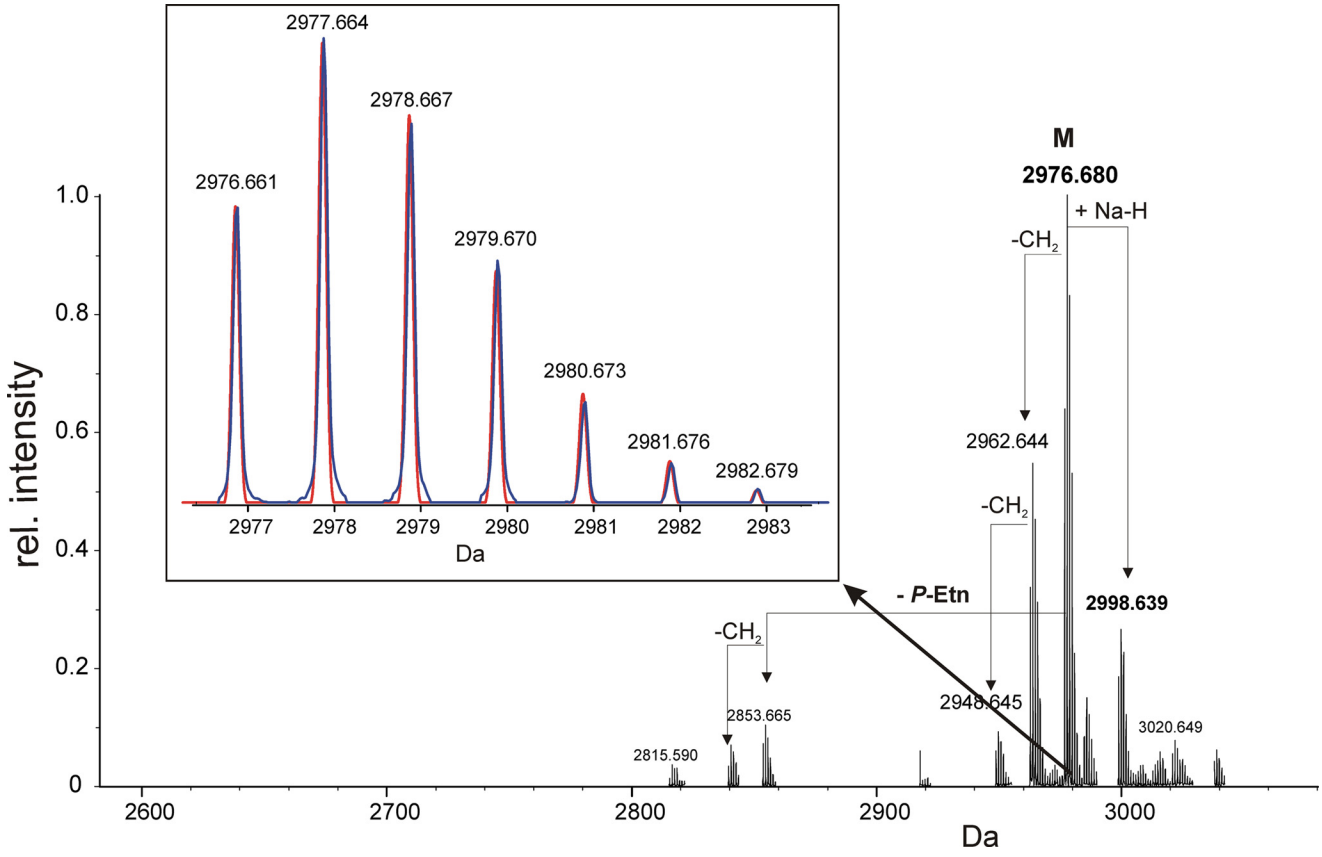

FIGURE 3. **Charge-deconvoluted mass spectrum of 3 obtained by ESI Fourier transform ion cyclotron resonance MS in the negative ion mode.** The monoisotopic mass found (2976.680 Da) is in excellent agreement with structure **3** (Fig. 1). The inlet shows an enlargement of the isotopic peaks obtained from the most abundant peak. The calculated ion intensity profile (*red*) is nearly identical to the measured one (*blue*), indicating the heterogeneity in the hybrid lipid A backbone (GlcN3N-GlcN) *versus E. coli*-type backbone (GlcN-GlcN) to be minor (~1–2%). Mass values in the *inset* represent the calculated masses for **3**.

Another advantage of this approach is the fact that, after extensive and non-destructive NMR analysis, the LPS preparation under investigation remains available for further biological studies.

In order to demonstrate the feasibility and power of this NMR method, we have chosen a rough-type LPS of *C. canimorsus*, the lipid A structure and biological (endotoxic) activities of which have recently been described (11). In this previous study, only the lipid A and not the structures of the core oligosaccharide (**1**) and the complete rough-type LPS (**3**) were analyzed. In the present study, we aim to close this gap. We could confirm the impact of our method in comparing it with the classical way

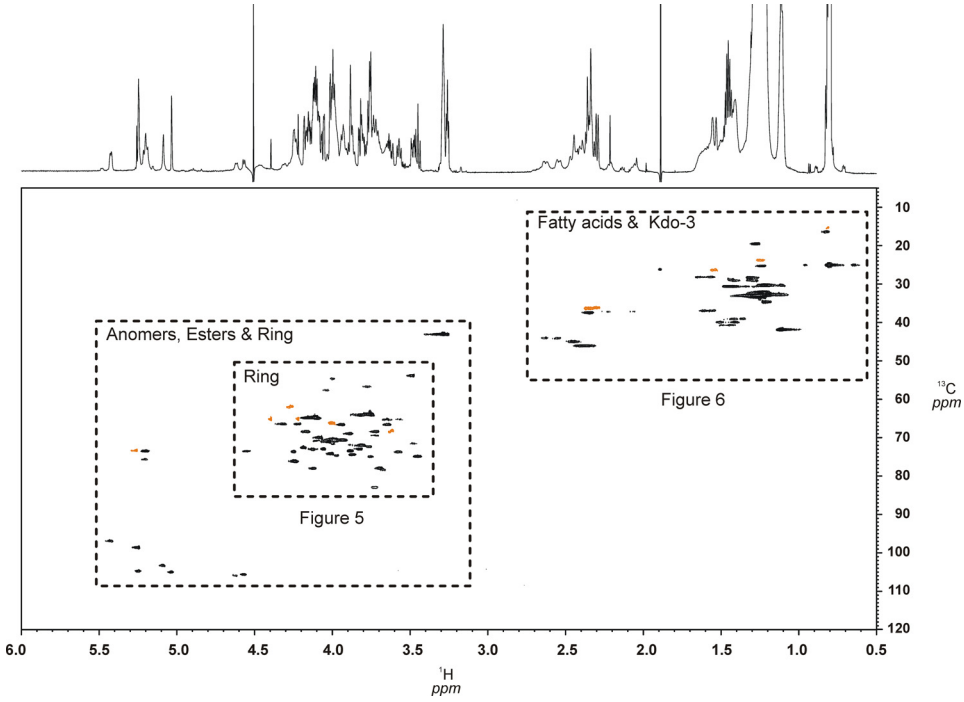

FIGURE 4. **HSQC-contour plot of the complete spectrum (^{1}H 6.0–0.5 ppm, ^{13}C 120–5 ppm) in which all three distinct regions of 3 can be clearly distinguished.** Ring protons/carbon signals and those of fatty acids are enlarged in Fig. 5 and 6, to demonstrate good signal resolution. Signals from the DHPC-d_{40} (98% D) detergent are shown in *orange*. The ^{1}H NMR spectrum is shown along the F2 axis at the *top*.

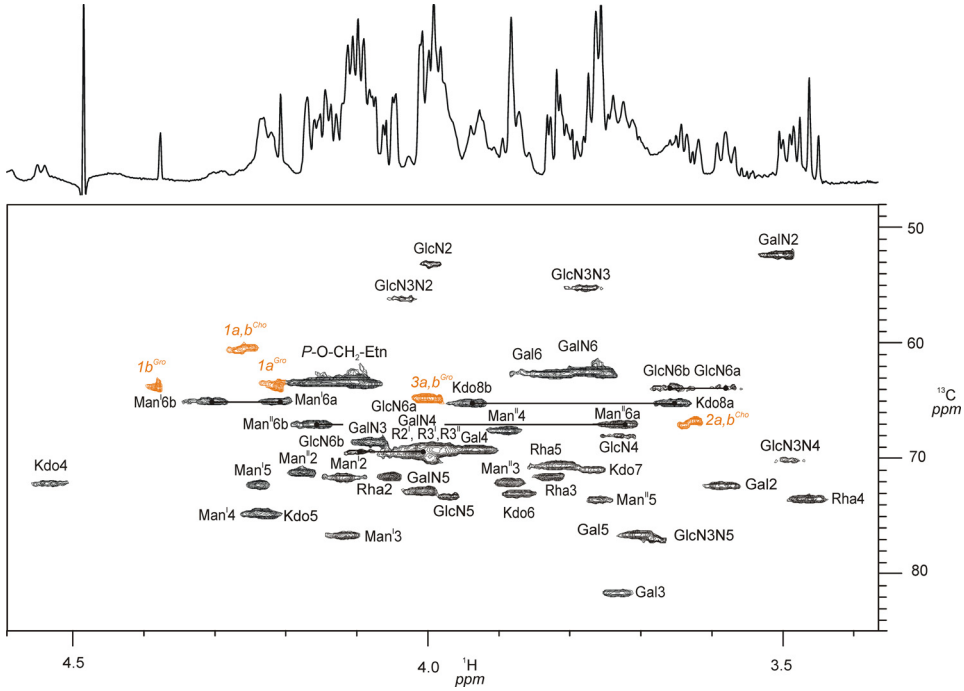

FIGURE 5. **Section of the ^{1}H,^{13}C-HSQC NMR (700 MHz) spectrum showing ring proton/carbon signals of 3.** The spectrum was recorded at 325 K in D_2O containing 1.5% DHPC-d_{40}. Selected ^{1}H,^{13}C ring signals and their assignments are indicated. ^{1}H,^{13}C signals from the DHPC-d_{40} detergent (98% D) are shown in *orange*. The one-dimensional ^{1}H spectrum is shown as a projection of the F2 axis.

of determining the core oligosaccharide by cleaving the LPS molecule in two parts and separating the resulting core oligosaccharide from the water-insoluble free lipid A. After mild acid treatment, a hexasaccharide (1) could be isolated in pure form. In a second approach, strong hydrazinolysis to deacylate the LPS revealed an octasaccharide (2), representing the carbohydrate part of the rough-type LPS (core oligosaccharide with a hybrid lipid A backbone (Glc*p*N3N-Glc*p*N) attached).

We also detected trace amounts (1–2%) of the *E. coli*-type backbone (Glc*p*N-Glc*p*N). This lipid A backbone type has also been found in the LPS of *Flavobacterium meningosepticum*, representing another species of *Flavobacteriaceae* to which *C. canimorsus* belongs. However, in *F. menigosepticum*, the

TABLE 4
^{1}H and ^{13}C NMR data of the fatty acids in 3
Data were taken from HSQC spectra. Signals of C-1 carbons are not indicated.

Proton	δ_H (ppm)	Carbon	δ_C (ppm)
Residue			
R2	*i*17:0(3-OH)		
H-2a	2.45	C-2	44.9
H-2b	2.45		
H-3	4.02	C-3	69.3
H-4a	1.43	C-4	38.7
H-4b	1.43		
H-5a,b.	1.22	C-5	28.3
H-6 ... H-13	1.10 ... 1.35	C-6 ... C-13	30 ... 31
H14a,b	1.11	C-14	39.9
H-15	1.43	C-15	28.6
H-15Me	0.80	C-15Me	23.2
H-16	0.80	C-16	23.2
R3	*i*15:0(3-OH)		
H-2a	2.54	C-2	42.0
H-2b	2.64		
H-3	3.99	C-3	69.2
H-4a	1.55	C-4	35.0
H-4b	1.61		
H-5a.	1.21	C-5	28.8
H-5b	1.43		
H-6 ... H-11	1.10 ... 1.35	C-6 … C13	30 ... 31
H-12	1.11	C-12	39.9
H-13	1.21	C-13	28.4
H-13Me	0.80	C-13Me	23.2
H-14	0.80	C-14	23.2
R2'	*i*17:0(3-OH)		
H-2a	2.34	C-2	44.9
H-2b	2.41		
H-3	5.20	C-3	74.0
H-4a	1.40	C-4	38.1
H-4b	1.51		
H-5a,b.	1.22	C-5	28.3
H-6 ... H-13	1.10 ... 1.35	C-6 … C13	30 ... 31
H-14a,b	1.11	C-14	39.9
H-15	1.43	C-15	28.6
H-15Me	0.80	C-15Me	23.0
H-16	0.80	C-16	23.0
R2''	*i*15:0		
H-2a,b	2.34	C-2	35.6
H-3a,b	1.57,1.65	C-3	26.4
H-4a,b	1.21	C-4	31.6
H-5...11	1.10 ... 1.35	C-5 ... C-11	30 ... 31
H-12a,b	1.11	C-12	39.9
H-13a,b	1.21	C-13	28.4
H-13Me	0.80	C-13Me	23.2
H-14	0.80	C-14	23.2
R3'	16:0(3-OH)		
H-2a	2.34	C-2	44.1
H-2b	2.41		
H-3	3.99	C-3	69.2
H-4a	1.55	C-4	35.0
H-4b	1.61		
H-5a,b	1.30	C-5	26.4
H-6 ... H13	1.10 ... 1.35	C-6 … C13	30 ... 31
H-14a,b	1.13	C-14	26.2
H-15a,b	1.24	C-15	23.3
H-16	0.82	C-16	14.6

E. coli-type backbone dominated, and the proportion of both lipid A backbones was inverted (38), thus being different from the lipid A backbone identified here.

Both oligosaccharides **1** and **2** have been extensively analyzed by NMR spectroscopy. Because NMR spectra for **3** were also recorded in water, a direct comparison of the NMR resonances from all ^{1}H,^{13}C and ^{31}P signals (and even, in some cases, coupling constants of ^{1}H signals ($^{3}J_{n,n+1}$)) could be made. In addition, the comparability of NMR data facilitates further LPS structural analysis considerably, because many NMR data of various linear and branched polysaccharides are referenced and available via internet databases and utilities (*e.g.* CASPER) (39).

Phosphorylation of Kdo at position C-4 appears not to be unique for *C. canimorsus*, where it is present in its *P*-Etn form. It is also found in core oligosaccharides from other Gram-negative bacteria, such as *Haemophilus influenzae* I-69 (40) and in non-typeable *H. influenzae*, where this position of Kdo carries a pyrophosphoethanolamine residue (41). Additionally, such phosphorylation has been identified in the inner core oligosaccharide of *Bordetella pertussis* (42) and *Vibrio cholerae* (43). The 4-*P* at Kdo^{I} can, by means of charge, replace the carboxyl group of the second Kdo (Kdo^{II}), usually present in the LPS of *Enterobacteriaceae*. This second negative charge represents an important and conserved structural feature in nearly all Gram-negative bacteria. However, in the case of *C. canimorsus* LPS, the 4-*P* does not contribute to the second negative charge because of its positively charged Etn substituent.

We expected that the zwitterionic residues of *P*-Etn at C-4 of Kdo may influence the conformation of the oligosaccharide considerably, both in the free oligosaccharide forms (**1** and **2**) and in complete rough-type LPS (**3**). Diagnostic NOEs were found to be indicative of different conformers, which are influenced by zwitterionic interactions, because they also influence the freedom in adopting various conformations of this branched core hexasaccharide. Such specific NOEs are shown in Figs. 7 and 8, and corresponding NMR data are given in Table 2. Surprisingly, we found a high flexibility for the core oligosaccharide even when attached to the lipid A anchor, which is expected to refit the conformational freedom of the inner core oligosaccharide when embedded via the lipid A anchor into the bacterial outer membrane. The spectrum and interpretation of the ROESY signals given in Fig. 8 show one extremely distorted conformer. It is most likely that this conformational freedom of the core oligosaccharide is also realized in case where the LPS molecule is located in the outer leaflet of the outer bacterial membrane.

In agreement with the x-ray crystallographic data, this extreme kind of conformational freedom of the core oligosaccharide in the native form is advantageous for a specific interaction of charged and polar groups of the LPS with those in the corresponding endotoxin target proteins, such as MD-2, TLR4, CD-14, and LBP (17). But most interestingly, this special role of the core oligosaccharide for endotoxin/receptor interaction cannot be observed by x-ray crystallographic studies. NMR conformational analysis, as used here, might be considered to represent a complementary method to investigate carbohydrate conformations and dynamics, which has not been possible to describe in detail so far in these molecules (17, 44, 45).

Recently, we published the structure-function analysis of lipid A isolated from the LPS of *C. canimorsus* 5 and found that this lipid A is penta-acylated and lacks the 4′-phosphate in the hybrid lipid A backbone (11). Because the 4′-phosphate-deprived lipid A is known to reduce the endotoxic activity significantly (12), we here try to describe a model that can explain why the *C. canimorsus* LPS nevertheless is able to induce an overwhelming sepsis. The impact for endotoxicity of this negatively charged 4′-phosphate came from data obtained by x-ray crystallography on the TLR4·MD-2·LPS complex (17) as well as from functional studies (46) and genome-wide profiling (47). This ionic interaction is important because it is critical for the ligand affinity of lipid A, enabling formation of a hexameric $(TLR4{\cdot}MD\text{-}2{\cdot}LPS)_2$ complex, which is necessary for TLR4-me-

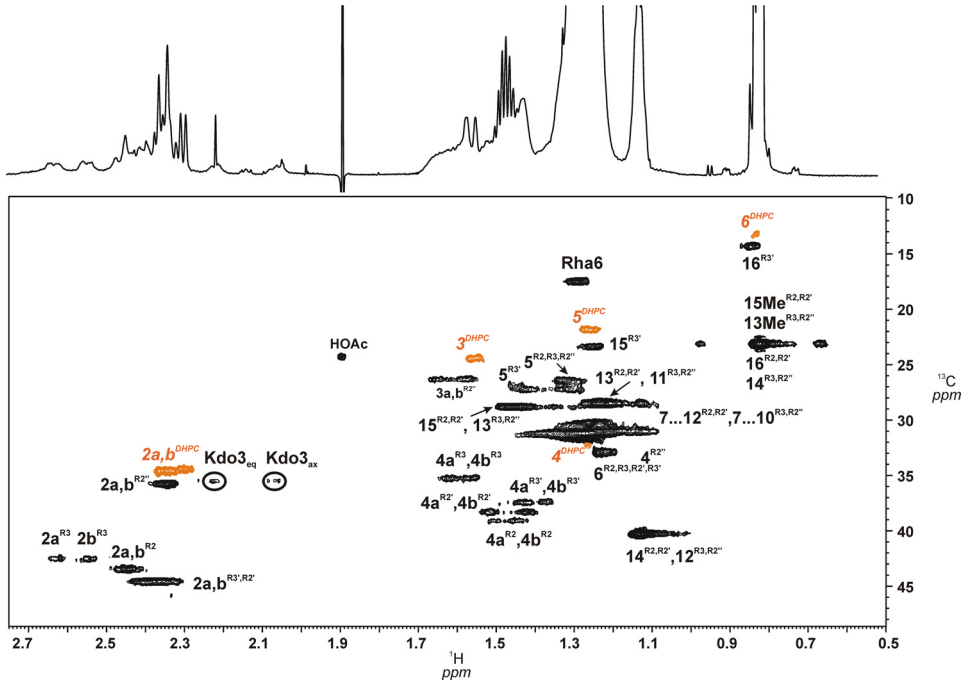

FIGURE 6. **HSQC contour plot showing the region with fatty acid signals H-2/C-2 to H-ω/C-ω as well as H-3$_{ax,eq}$/C-3 Kdo and H-6/C-6 of L-Rha sugars.** Signals assigned to one acyloxyacyl residue (R2″-R2′), (3*R*)-3-(15-methyl-hexadecanoyloxy)-13-methyl-tetradecanoic acid, attached to position 2′ of Glc*p*N3N (II) as well as those originating from the (*R*)-3-hydroxy-hexadecanoic acid (R3′) are indicated. Signals from the DHPC-d_{40} detergent are shown in *orange*.

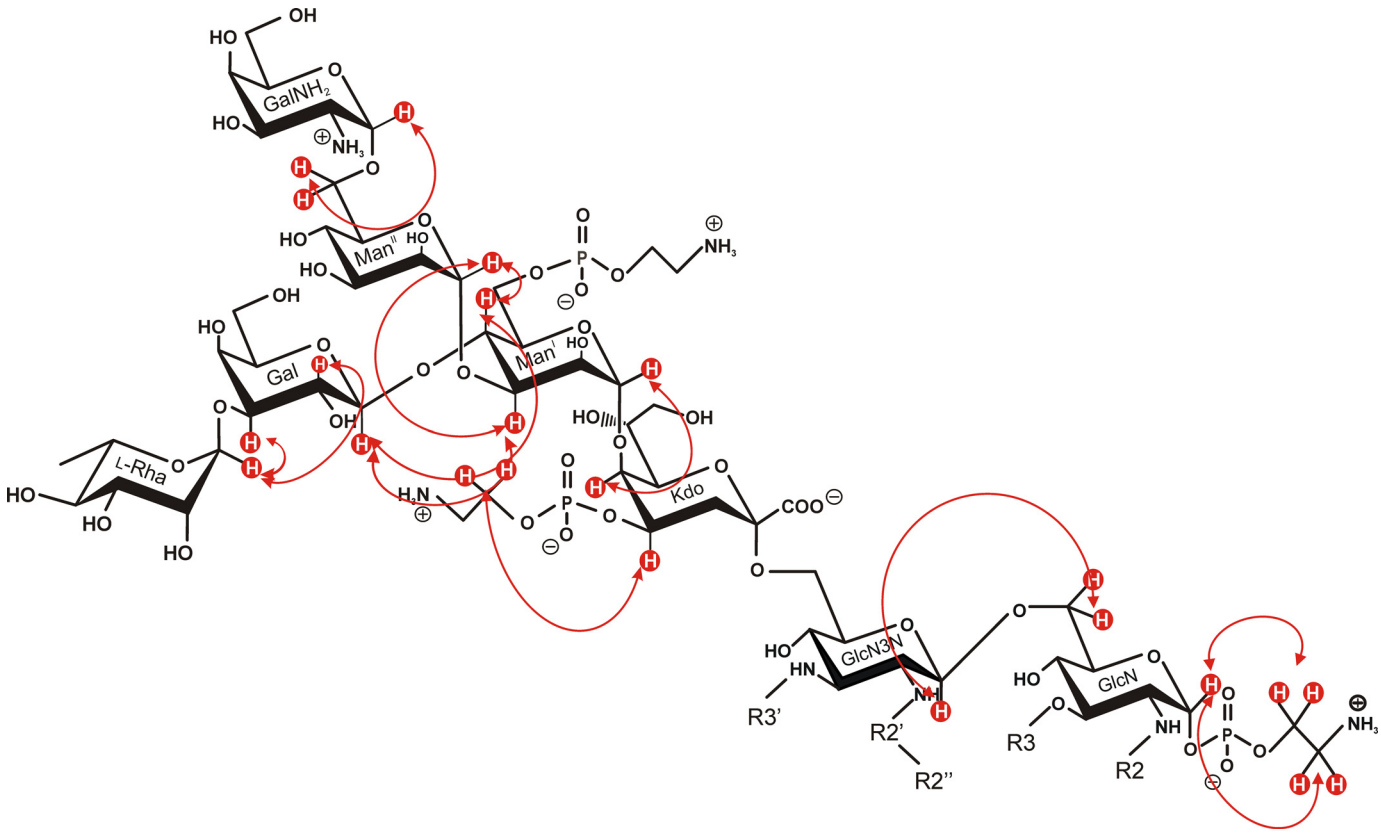

FIGURE 7. **NOE connectivities detected in 3 by which the linkages of sugars and *P*-Etn residues were assigned.** Some of the anomeric protons (*e.g.* H-1 of L-Rha and Man^{II}) show NOE cross-peaks (Table 2) not only to the substituting but also to the neighboring sugar protons to which they are bound, indicating a rather twisted conformation of the branched oligosaccharide. The fatty acid residues attached to the lipid A backbone (R3′, R2″-R2′, R3, and R2) are abbreviated for clarity.

diated signaling. Therefore, we raised the question of whether the negatively charged carboxylate group in position C-1 of the Kdo might be able to substitute the lacking 4′-phosphate in the lipid A backbone. This assumption is based on the complex model of Park *et al.* (17) as well as our own modeling calculations (11).

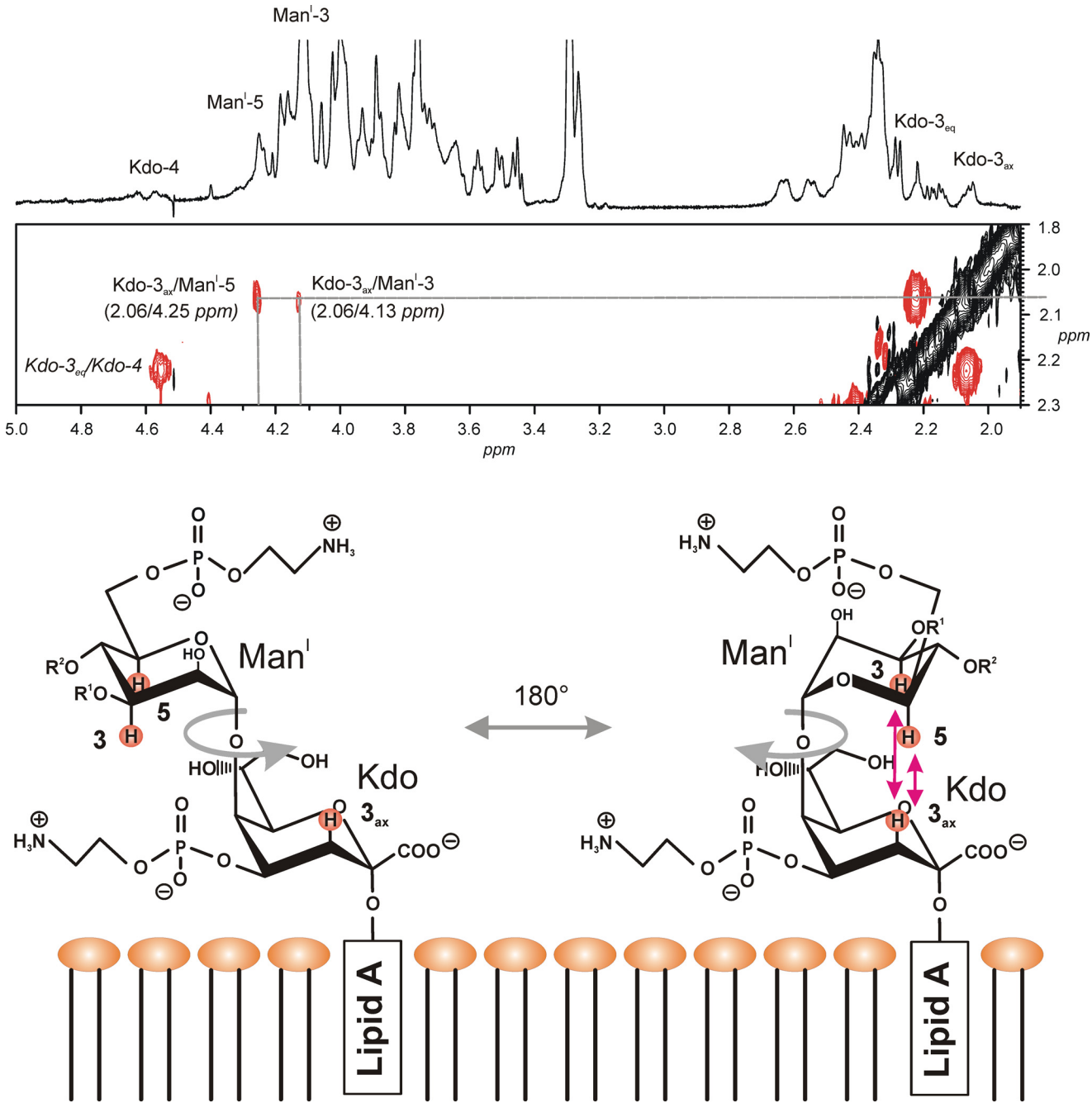

FIGURE 8. **Special conformation adopted by the intact core when bound to the lipid A.** Shown is part of the ROESY spectrum of **3** with NOE signals showing interresidual connectivities between H-3$_{ax}$ of Kdo and H-3/H-5 of Man^{I}. This indicates a free rotation in the core oligosaccharide of about 180° (*gray arrow*) around the Man^{I}-C1-O-C5-Kdo bond axis as shown in the *bottom part* together with the membrane matrix of the DHPC micelles. Indicated are the two disaccharides attached to Man^{I} (*i.e.* α-L-Rha*p*-(1→3)-β-D-Gal*p*-(1→ (*OR*^{1}) and α-D-GalN*p*-(1→6)-α-D-Man*p*^{II}-(1→4) (*OR*^{2})).

We concluded that the negatively charged carboxyl group at C-1 of the Kdo can adopt the function of the negative charge of the 4′-*P* attached to the non-reducing part of the lipid A backbone. Based on our model, the lacking 4′-*P* and, hence, its negative charge can be structurally and functionally replaced by the carboxy group of Kdo, this way resuming the electrostatic binding to the positively charged amino acids identified for binding to TLR4 (Arg-264 and Lys-362) and MD-2 (Ser-118 and Lys-58) (Protein Data Bank code 3FXI) (17). The importance of the charged groups for LPS·TLR4·MD-2 has also been identified by Meng *et al.* (46) for the binding of lipid IV$_{A}$ to MD-2 and TLR4. Molecular modeling revealed that this negative charge might indeed be an essential structural feature for this kind of binding (core oligosaccharide to MD-2 (11)). Notably, in human MD-2, three positively charged amino acids (Lys-122, Lys-125, and Lys-58) have been identified by functional studies to be important for TLR4-independent LPS recognition by MD-2. Of these, Lys-58 is in spatial proximity to the 4′-*P* of the lipid A backbone. We have previously shown by molecular modeling that *C. canimorsus* lipid A is probably binding to human MD-2 in a very similar way as *E. coli* hexa-acylated lipid A (11). This further supports the idea that the negatively charged carboxylate group

of the proximate Kdo may indeed compensate for the lack of the 4′-*P* in the lipid A backbone of *C. canimorsus* (48). The outcome of this ionic compensation might explain the strongly enhanced endotoxic activity, when comparing *C. canimorsus* free lipid A with rough-type LPS, differing by a factor of 20,000 (11). The fact that the negative charge of a carboxymethyl group in lipid A indeed can mimic that of a phosphate residue has been shown for different synthetic lipid A structures (49), further supporting our interpretation.

In this context, another important structural feature of the rough-type LPS of *C. canimorsus* deserves special mention. The innate immune defense takes advantage of antimicrobial peptides (AMPs), which represent one of the first lines of defense against pathogenic bacteria. AMPs are present in phagocytic cells on body surfaces, skin, and mucosa (50). In most cases, AMPs represent positively charged peptides and act as neutralizing agents able to kill bacterial pathogens by insertion into the membrane and disruption (51). The main targets of AMPs in Gram-negative bacteria, therefore, are negatively charged polar lipids on the surface of the bacterial outer membrane, especially LPS (52). However, due to the zero net charge of the LPS/lipid A structure described here, *C. canimorsus* is able to avoid this kind of ionogenic attack by AMPs. Therefore, this structural element provides an advantage against immunological defense based on positively charged antimicrobial peptides secreted by the host, especially in the dog's mouth, which represents the natural habitat of *C. canimorsus* bacteria.

Acknowledgments—We are thankful to Y. A. Knirel, O. Bystrova, and E. Zdorovenko (N. D. Zelinsky Institute, Moscow, Russia) for assistance at the beginning of the project; E. Vinogradov (National Research Council, Ottawa, Canada) for help with interpretation of NMR spectra; and S. Meier (Department of Chemistry, Technical University of Denmark, Lyngby, Denmark) for critically reading the manuscript. The skillful assistance of B. Kunz with ESI-MS analysis is also gratefully acknowledged.

REFERENCES

1. Oehler, R. L., Velez, A. P., Mizrachi, M., Lamarche, J., and Gompf, S. (2009) Bite-related and septic syndromes caused by cats and dogs. *Lancet Infect. Dis.* **9,** 439–447
2. Janda, J. M., Graves, M. H., Lindquist, D., and Probert, W. S. (2006) Diagnosing *Capnocytophaga canimorsus* infections. *Emerg. Infect. Dis.* **12,** 340–342
3. Shin, H., Mally, M., Kuhn, M., Paroz, C., and Cornelis, G. R. (2007) Escape from immune surveillance by *Capnocytophaga canimorsus*. *J. Infect. Dis.* **195,** 375–386
4. Mally, M., Paroz, C., Shin, H., Meyer, S., Soussoula, L. V., Schmiediger, U., Saillen-Paroz, C., and Cornelis, G. R. (2009) Prevalence of *Capnocytophaga canimorsus* in dogs and occurrence of potential virulence factors. *Microbes Infect.* **11,** 509–514
5. Pers, C., Gahrn-Hansen, B., and Frederiksen, W. (1996) *Capnocytophaga canimorsus* septicemia in Denmark, 1982–1995: review of 39 cases. *Clin. Infect. Dis.* **23,** 71–75
6. Mally, M., Shin, H., Paroz, C., Landmann, R., and Cornelis, G. R. (2008) *Capnocytophaga canimorsus*: a human pathogen feeding at the surface of epithelial cells and phagocytes. *PLoS Pathog.* **4,** e1000164
7. Manfredi, P., Renzi, F., Mally, M., Sauteur, L., Schmaler, M., Moes, S., Jenö, P., and Cornelis, G. R. (2011) The genome and surface proteome of *Capnocytophaga canimorsus* reveal a key role of glycan foraging systems in host glycoproteins deglycosylation. *Mol. Microbiol.* **81,** 1050–1060
8. Renzi, F., Manfredi, P., Mally, M., Moes, S., Jenö, P., and Cornelis, G. R. (2011) The *N*-glycan glycoprotein deglycosylation complex (Gpd) from *Capnocytophaga canimorsus* deglycosylates human IgG. *PLoS Pathog.* **7,** e1002118
9. Shin, H., Mally, M., Meyer, S., Fiechter, C., Paroz, C., Zaehringer, U., and Cornelis, G. R. (2009) Resistance of *Capnocytophaga canimorsus* to killing by human complement and polymorphonuclear leukocytes. *Infect. Immun.* **77,** 2262–2271
10. Alexander, C., and Rietschel, E. T. (2001) Bacterial lipopolysaccharides and innate immunity. *J. Endotoxin Res.* **7,** 167–202
11. Ittig, S., Lindner, B., Stenta, M., Manfredi, P., Zdorovenko, E., Knirel, Y. A., dal Peraro, M., Cornelis, G. R., and Zähringer, U. (2012) The lipopolysaccharide from *Capnocytophaga canimorsus* reveals an unexpected role of the core-oligosaccharide in MD-2 binding. *PLoS Pathog.* **8,** e1002667
12. Loppnow, H., Brade, H., Dürrbaum, I., Dinarello, C. A., Kusumoto, S., Rietschel, E. T., and Flad, H.-D. (1989) IL-1 induction-capacity of defined lipopolysaccharide partial structures. *J. Immunol.* **142,** 3229–3238
13. Rietschel, E. T., Kirikae, T., Schade, F. U., Mamat, U., Schmidt, G., Loppnow, H., Ulmer, A. J., Zähringer, U., Seydel, U., Di Padova, F. (1994) Bacterial endotoxin: molecular relationships of structure to activity and function. *FASEB J.* **8,** 217–225
14. Zähringer, U., Lindner, B., and Rietschel, E. T. (1999) Chemical structure of lipid A: recent advances in structural analysis of biologically active molecules. Brade, H., Opal, S., Vogel, S., and Morrison, D. C. (eds) *Endotoxin in Health and Disease*, pp. 93–114, Marcel Dekker, New York
15. Raetz, C. R. H., Garrett, T. A., Reynolds, C. M., Shaw, W. A., Moore, J. D., Smith, D. C., Jr., Ribeiro, A. A., Murphy, R. C., Ulevitch, R. J., Fearns, C., Reichart, D., Glass, C. K., Benner, C., Subramaniam, S., Harkewicz, R., Bowers-Gentry, R. C., Buczynski, M. W., Cooper, J. A., Deems, R. A., and Dennis, E. A. (2006) Kdo_2-Lipid A of *Escherichia coli*, a defined endotoxin that activates macrophages via TLR-4. *J. Lipid Res.* **47,** 1097–1111
16. Richter, W., Vogel, V., Howe, J., Steiniger, F., Brauser, A., Koch, M. H. J., Roessle, M., Gutsmann, T., Garidel, P., Mäntele, W., and Brandenburg, K. (2011) Morphology, size distribution, and aggregate structure of lipopolysaccharide and lipid A dispersions from enterobacterial origin. *Innate Immun.* **17,** 427–438
17. Park, B. S., Song, D. H., Kim, H. M., Choi, B.-S., Lee, H., and Lee, J.-O. (2009) The structural basis of lipopolysaccharide recognition by the TLR4-MD-2 complex. *Nature* **458,** 1191–1195
18. DeMarco, M. L., and Woods, R. J. (2011) From agonist to antagonist: structure and dynamics of innate immune glycoprotein MD-2 upon recognition of variably acylated bacterial endotoxins. *Mol. Immunol.* **49,** 124–133
19. Westphal, O., and Jann, K. (1965) Bacterial lipopolysaccharides. Extraction with phenol-water and further applications of the procedure. *Methods Carbohydr. Chem.* **5,** 83–91
20. Galanos, C., Lüderitz, O., and Westphal, O. (1969) A new method for the extraction of R lipopolysaccharides. *Eur. J. Biochem.* **9,** 245–249
21. Vinogradov, E., Perry, M. B., and Conlan, J. W. (2002) Structural analysis of *Francisella tularensis* lipopolysaccharide. *Eur. J. Biochem.* **269,** 6112–6118
22. Kawai, Y., Yano, I., and Kaneda, K. (1988) Various kinds of lipoamino acids including a novel serine-containing lipid in an opportunistic pathogen *Flavobacterium*: their structure and biological activities on erythrocytes. *Eur. J. Biochem.* **171,** 73–80
23. Godchaux, W., 3rd, and Leadbetter, E. R. (1980) *Capnocytophaga* spp. contain sulfonolipids that are novel in procaryotes. *J. Bacteriol.* **144,** 592–602
24. Godchaux, W., 3rd, and Leadbetter, E. R. (1984) Sulfonolipids of gliding bacteria. Structure of the *N*-acylaminosulfonates. *J. Biol. Chem.* **259,** 2982–2990
25. Caroff, M., Tacken, A., and Szabó, L. (1988) Detergent-accelerated hydrolysis of bacterial endotoxins and determination of the anomeric configuration of the glycosyl phosphate present in the "isolated lipid A" fragment of the *Bordetella pertussis* endotoxin. *Carbohydr. Res.* **175,** 273–282
26. Laemmli, U. K. (1970) Cleavage of structural proteins during the assembly of the head of bacteriophage T4. *Nature* **227,** 680–685
27. Tsai, C. M., and Frasch, C. E. (1982) A sensitive silver stain for detecting

lipopolysaccharides in polyacrylamide gels. *Anal. Biochem.* **119,** 115–119
28. Leontein, K., Lindberg, B., and Lönngren, J. (1978) Assignment of absolute configuration of sugars by g.l.c. of their acetylated glycosides formed from chiral alcohols. *Carbohydr. Res.* **62,** 359–362
29. Hase, S., and Rietschel, E. T. (1976) Isolation and analysis of the lipid A backbone. Lipid A structure of lipopolysaccharides from various bacterial groups. *Eur. J. Biochem.* **63,** 101–107
30. Pitta, T. P., Leadbetter, E. R., and Godchaux, W., 3rd (1989) Increase of ornithine amino lipid content in a sulfonolipid-deficient mutant of *Cytophaga johnsonae*. *J. Bacteriol.* **171,** 952–957
31. Gomi, K., Kawasaki, K., Kawai, Y., Shiozaki, M., and Nishijima, M. (2002) Toll-like receptor 4-MD-2 complex mediates the signal transduction induced by flavolipin, an amino acid-containing lipid unique to *Flavobacterium meningosepticum*. *J. Immunol.* **168,** 2939–2943
32. Wang, W., Sass, H.-J., Zähringer, U., and Grzesiek, S. (2008) Structure and dynamics of ^{13}C,^{15}N-labeled lipopolysaccharide in a membrane mimetic. *Angew. Chem. Int. Ed. Engl.* **47,** 9870–9874
33. Zähringer, U., Sinnwell, V., Peter-Katalinic, J., Rietschel, E. T., and Galanos, C. (1993) Isolation and characterization of the tetrasaccharide (bis)-phosphate from the glycosyl backbone of *Salmonella minnesota* and *Escherichia coli* Re-mutant lipopolysaccharides. *Tetrahedron* **49,** 4193–4200
34. Moll, H., Knirel, Y. A., Helbig, J. H., and Zähringer, U. (1997) Identification of an α-D-Man*p*-(1→8)-Kdo disaccharide in the inner core region and the structure of the complete core region of the *Legionella pneumophila* serogroup 1 lipopolysaccharide. *Carbohydr. Res.* **304,** 91–95
35. Kondakova, A., and Lindner, B. (2005) Structural characterization of complex bacterial glycolipids by Fourier transform mass spectrometry. *Eur. J. Mass Spectrom.* **11,** 535–546
36. Kohara, J., Tsuneyoshi, N., Gauchat, J.-F., Kimoto, M., and Fukudome, K. (2006) Preparation and characterization of truncated human lipopolysaccharide-binding protein in *Escherichia coli*. *Protein Expr. Purif.* **49,** 276–283
37. Kim, J.-I., Lee, C. J., Jin, M. S., Lee, C.-H., Paik, S.-G., Lee, H., and Lee, J.-O. (2005) Crystal structure of CD14 and its implications for lipopolysaccharide signaling. *J. Biol. Chem.* **280,** 11347–11351
38. Kato, H., Haishima, Y., Iida, T., Tanaka, A., and Tanamoto, K. (1998) Chemical structure of lipid A isolated from *Flavobacterium meningosepticum* lipopolysaccharide. *J. Bacteriol.* **180,** 3891–3899
39. Jansson, P. E., Kenne, L., and Widmalm, G. (1989) Computer-assisted structural analysis of polysaccharides with an extended version of casper using ^{1}H- and ^{13}C-n.m.r. data. *Carbohydr. Res.* **188,** 169–191
40. Helander, I. M., Lindner, B., Brade, H., Altmann, K., Lindberg, A. A., Rietschel, E. T., and Zähringer, U. (1988) Chemical structure of the lipopolysaccharide of *Haemophilus influenzae* strain I-69 Rd^{-}/b^{+}: Description of a novel deep-rough chemotype. *Eur. J. Biochem.* **177,** 483–492
41. Schweda, E. K. H., Twelkmeyer, B., and Li, J. (2008) Profiling structural elements of short-chain lipopolysaccharide of non-typeable *Haemophilus influenzae*. *Innate Immun.* **14,** 199–211
42. Lebbar, S., Caroff, M., Szabó, L., Mérienne, C., and Szilógyi, L. (1994) Structure of a hexasaccharide proximal to the hydrophobic region of lipopolysaccharides present in *Bordetella pertussis* endotoxin preparations. *Carbohydr. Res.* **259,** 257–275
43. Bock, K., Vinogradov, E. V., Holst, O., and Brade, H. (1994) Isolation and structural analysis of oligosaccharide phosphates containing the complete carbohydrate chain of the lipopolysaccharide from *Vibrio cholerae* strain H11 (non-O1). *Eur. J. Biochem.* **225,** 1029–1039
44. Ohto, U., Fukase, K., Miyake, K., and Satow, Y. (2007) Crystal structures of human MD-2 and its complex with antiendotoxic lipid IVa. *Science* **316,** 1632–1634
45. Kim, H. M., Park, B. S., Kim, J.-I., Kim, S. E., Lee, J., Oh, S. C., Enkhbayar, P., Matsushima, N., Lee, H., Yoo, O. J., and Lee, J.-O. (2007) Crystal structure of the TLR4-MD-2 complex with bound endotoxin antagonist Eritoran. *Cell* **130,** 906–917
46. Meng, J., Lien, E., and Golenbock, D. T. (2010) MD-2-mediated ionic interactions between lipid A and TLR4 are essential for receptor activation. *J. Biol. Chem.* **285,** 8695–8702
47. Meng, J., Gong, M., Björkbacka, H., and Golenbock, D. T. (2011) Genome-wide expression profiling and mutagenesis studies reveal that lipopolysaccharide responsiveness appears to be absolutely dependent on TLR4 and MD-2 expression and is dependent upon intermolecular ionic interactions. *J. Immunol.* **187,** 3683–3693
48. Vasl, J., Oblak, A., Gioannini, T. L., Weiss, J. P., and Jerala, R. (2009) Novel roles of lysines 122, 125, and 58 in functional differences between human and murine MD-2. *J. Immunol.* **183,** 5138–5145
49. Liu, W. C., Oikawa, M., Fukase, K., Suda, T., and Kusumoto, S. (1999) A divergent synthesis of lipid A and its chemically stable unnatural analogues. *Bull. Chem. Soc. Jpn.* **72,** 1377–1385
50. Gruenheid, S., and Le Moual, H. (2012) Resistance to antimicrobial peptides in Gram-negative bacteria. *FEMS Microbiol. Lett.* **330,** 81–89
51. Hancock, R. E. W., and Sahl, H.-G. (2006) Antimicrobial and host-defense peptides as new anti-infective therapeutic strategies. *Nat. Biotechnol.* **24,** 1551–1557
52. Chamorro, C., Boerman, M. A., Arnusch, C. J., Breukink, E., and Pieters, R. J. (2012) Enhancing membrane disruption by targeting and multicalent presentation of antimicrobial peptides. *Biochim. Biophys. Acta* **1818,** 2171–2174